




# Making liquid crystals twitch under metamaterial-enhanced terahertz illumination: toward strong optical nonlinearity

**BEN BEDDOES,<sup>1,\*</sup>  NICHOLAS KLOKKOU,<sup>1</sup> MALGOSIA KACZMAREK,<sup>1</sup> VASSILI A. FEDOTOV,<sup>1</sup> AND VASILIS APOSTOLOPOULOS<sup>1,2,3</sup> **

<sup>1</sup>*Physics and Astronomy, University of Southampton, Highfield SO17 1BJ, UK*

<sup>2</sup>*University of Crete, Department of Physics, Heraklion GR-70013, Greece*

<sup>3</sup>*Foundation for Research and Technology-Hellas, Institute of Electronic Structure and Laser, Heraklion, Crete, Greece*

\**B.Beddoes@soton.ac.uk*

**Abstract:** We provide the first direct experimental evidence for the reorientation of liquid crystals by polarized radiation from a conventional, low power, oscillator-based terahertz time-domain spectrometer. Using a terahertz pump - optical probe setup, we observed that the reorientation occurs locally through the resonant amplification of the terahertz field in a specially designed planar metamaterial, adjacent to the liquid crystal layer, and increases with increasing incident terahertz intensity. Our work thus demonstrates that it is possible to induce strong optical nonlinearity in liquid crystals in the terahertz part of the spectrum, paving the way toward the development of new all-optical active terahertz devices as well as electric field sensors for localized resonant systems.

Published by Optica Publishing Group under the terms of the [Creative Commons Attribution 4.0 License](#). Further distribution of this work must maintain attribution to the author(s) and the published article's title, journal citation, and DOI.

## 1. Introduction

Terahertz (THz) technologies have attracted significant interest across various research fields including, but not limited to security [1], sensing [2] and imaging [3]. In particular, THz communication technologies are recognized as one of the key candidates for 6G networks due to their high speed, low latency and ultra-wideband characteristics [4–6]. This has led to a concerted effort toward the development of small, compact devices capable of efficiently manipulating free-space THz radiation [7,8]. However, conventional materials utilized in such devices often lack strong THz responses, posing a fundamental challenge in their development [9].

Metallic planar metamaterials (MMs) offer a promising solution to this challenge. They are represented by thin metal films patterned on a sub-wavelength scale, engineered to exhibit unique properties across a wide range of wavelengths. MMs enable the enhancement of diffraction-free light-matter interactions while maintaining a small device footprint [10,11]. To tune MM's resonant response, which is typically fixed after fabrication, MMs have been successfully integrated with liquid crystals (LCs), micro-electrical mechanical systems (MEMS), graphene, vanadium dioxide, and phase change materials, demonstrating dynamic THz modulation capabilities [11–15]. Such devices include ultra-broadband wave plates [16], dual-band absorbers [17], polarization converters and selectors [18,19], and programmable metasurfaces [4,10].

In a recent study of MM-enhanced LC cells, it has been suggested that the THz field generated by a conventional oscillator-based THz time-domain spectrometer (TDS), when incident upon such hybrid cells, may be sufficient to engage LC optical nonlinearity via an in-plane reorientation of the LC molecules [20]. It was hypothesized that the reorientation could be driven by the

incident THz field when resonantly amplified by the MM fabric. The validity of this claim was first confirmed in our subsequent theoretical study, whereby an in-plane switching (IPS) model of the  $K_2$  twist deformation of LCs was used to establish a theoretical framework for the proposed mechanism of reorientation [21]. In that study, the limits of reorientation were established namely that only a partial reorientation with a maximum twist of  $\frac{\pi}{4}$  would be achievable. This feature of our system ensures a non-zero twist angle for  $E \geq 0$ , lifting any restriction on the minimal strength of the electric field required to drive the LC reorientation and ensuring a thresholdless process. Furthermore, we would only expect a thin layer of 1  $\mu\text{m}$  above the metamaterials where this reorientation would occur, given by the  $1/e$  falloff of the in-plane electric field. Applying these limits, it was shown analytically that even a modest incident THz field, namely as low as 20 V/cm should be strong enough to affect the orientation of LC molecules. Such levels of electric field are achievable with most THz photo-conductive antennae (PCA) emitters as they typically operate in the 10-100 V/cm range [22].

In the work presented here, we prove experimentally using a THz pump optical probe setup, that the reorientation of LCs can indeed be induced by incident THz radiation in the presence of a specially designed metamaterial. The effect has been observed directly by measuring the optical transmission through the hybrid MM/LC cell when placed between polarizers. We also demonstrate that the degree of LC reorientation can be controlled by varying the intensity of THz radiation incident upon the hybrid cell. This was achieved by varying the bias voltage supplied to our PCA emitter. The resulting LC-based device can open up new research possibilities for all-optical switching technologies and other nonlinear studies in the THz regime that include near-field excitation of resonant systems. Furthermore, the LC molecules following the local electric field can be used as sensors which would give an intuitive mapping of the field distribution of a metasurface or other resonant systems. This would give a unique insight into localized nonlinearities in the THz regime.

## 2. Hybrid metamaterial-liquid crystal cells

In this study, we used 20  $\mu\text{m}$  thick LC optical cells integrated with a metallic planar MM based on D-shaped metamolecules [20], as shown in Fig. 1. This design was chosen to maximize the in-plane amplification of the THz field. The planar MM was fabricated by photolithographically etching a 300 nm layer of gold deposited on one of the quartz substrates of the hybrid cell, with a 5 nm chrome adhesion layer between the quartz and gold. Both the top and bottom substrates of the hybrid cell had a thin layer of PI deposited and mechanically rubbed to set the initial planar alignment of the LC director,  $\vec{n}$ , parallel to the straight sections of the metamolecules.

For this investigation, we used the highly birefringent LC 1825 [23], which reaches a  $\Delta n$  of 0.387 at 1 THz. Such highly birefringent, low-absorption LCs are critical for the realization of thin devices at THz frequencies, where the increased wavelength compared to visible light often necessitates the use of thick (several hundred microns) devices, resulting in slow switching times and increased cost [23]. By integrating highly birefringent LCs with MM films, we are able to reduce the layer thickness of THz LC devices to more efficient levels in line with typical visible light device thicknesses [10], which usually range between 1  $\mu\text{m}$  and 23  $\mu\text{m}$  [24,25].

The spectrum of a pristine MM exhibits a polarization-dependent Fano resonance [26], featuring a characteristic asymmetric profile when the THz field is polarized parallel to the straight sections of the metamolecules, see graph (blue line) inset to Fig. 1. For THz polarization perpendicular to the MM straight sections no such resonance is observed, see graph (orange line) inset Fig. 1. Fano resonances acquire their characteristic shape due to the excitation of the trapped mode within the metamolecules (also known as bound states in the continuum, BIC [27,28]), a weakly radiating mode, which corresponds to current oscillations in anti-phase between the two metamolecule sections (the "C" and the "I") [26]. For the D-shaped metamolecules used in our study, this results in local field enhancements of the input THz field by a factor exceeding

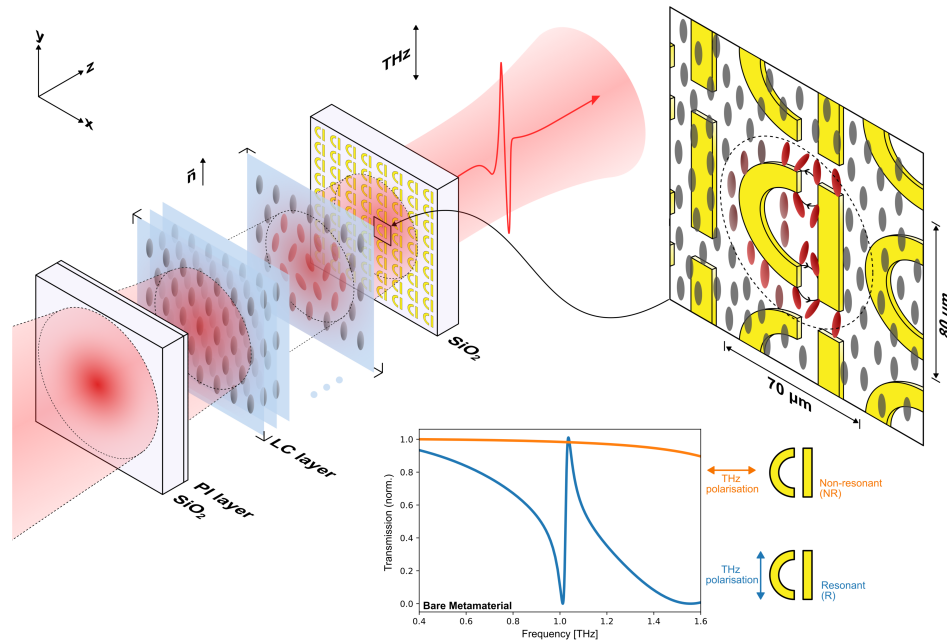


**Fig. 1.** A 3D representation of the hybrid LC/MM cell when resonant with the incident polarized THz field. Resonance (R) occurs when the THz radiation is polarized parallel to the straight segments of the metamolecules. When horizontally polarized THz is incident on the MMs, the system will be in the non-resonant (NR) condition and no amplification of the THz field will occur. See inset graph showing the resonance response of a bare metamaterial for horizontal (orange) and vertical (blue) THz polarization. LC reorientation is expected to be concentrated in a thin layer above the sharp geometric features of the metamolecules when in the resonant condition (see red LCs in the inset), as these ‘hotspots’ experience the highest in-plane amplification of the THz field by the MM fabric. LC molecules in these regions will reorient to follow the in-plane electric field of the MMs up to a maximum twist of  $\frac{\pi}{4}$ . Reorientation is not expected to continue through the entire  $20\ \mu\text{m}$  LC layer.  $\vec{n}$  denotes the LC director indicating the initial planar alignment direction. The inset dimensions show the size of the MM unit cell.

200 [20]. This phenomenon is underpinned by two combined effects: the amplification of the THz field by the metamolecules and the concentration of the electric field around their sharp geometric features [29,30].

The D-shaped MMs used in this investigation are designed to be diffraction-less when interacting with THz radiation [26]. However, the unit cell measuring  $70 \times 80\ \mu\text{m}$ , with  $10\ \mu\text{m}$  gaps, ensures that they do diffract visible light. Interestingly, bare MM samples with no LC layer will diffract linearly polarized visible light independently of the sample orientation. However, the introduction of a rubbed PI alignment layer and LCs creates a polarization-dependent diffraction pattern, as shown in Fig. 2(c). The orientation of visible light polarization is indicated by the white arrow.

Observation of the hybrid cell using a polarized microscope reveals elongated stripes that run parallel to the straight sections of the MMs when the incident visible light probes the long axis,  $n_e$  direction, of the LC molecules (see Fig. 2(b)). No such stripes are present when visible light probes the short axis of the LC molecules,  $n_o$  direction (see Fig. 2(a)). The alignment of these stripes also matches the rubbing direction of the PI used to set the initial alignment of the LCs. We hypothesize that these grooves are likely the result of interactions between the

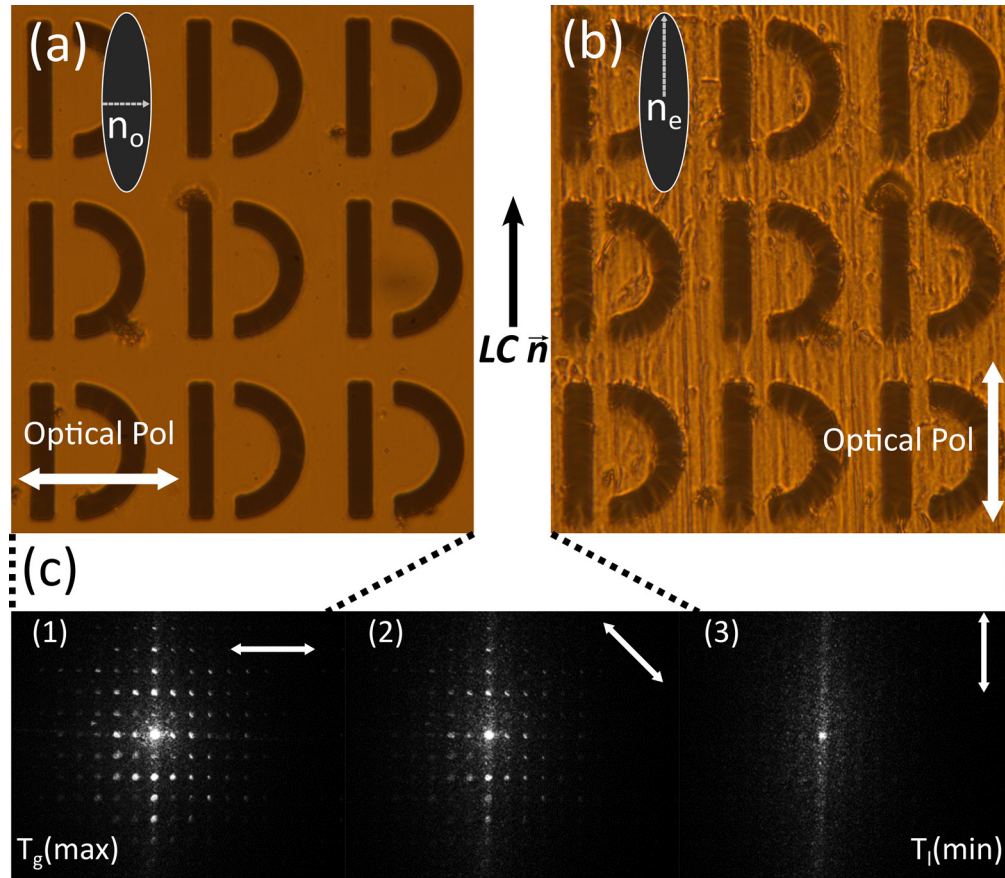


**Fig. 2.** Polarized optical microscope images of the hybrid MM/LC cell, with the rubbing direction and LC director (black arrow) parallel to the straight sections of the MMs. Each figure is taken without THz radiation incident on the sample. (a) Incident visible light polarized perpendicular to the MM straight edges (white arrow). For this orientation we are probing the short axis of the LCs ( $n_o$ ), which is unaffected by variations LC pretilt/anchoring in the  $n_e$  direction, hence a clear white light diffraction pattern is visible. (b) Incident visible light polarized parallel to the MM straight edges (white arrow). For this orientation we are probing the long axis of the LCs ( $n_e$ ) which is affected by pretilt/anchoring. For this configuration elongated stripes appear which we hypothesize are a result of the variations in pretilt/anchoring in the  $n_e$  direction, due to the MM structures. This disrupts the coherence of the diffraction pattern, causing it to disappear as depicted in (c), which shows the k-space images of the hybrid cell under white light illumination. As the polarization of the incident light is rotated from the configuration in (a) to (b), the diffraction pattern fades and eventually disappears.

MM structures (300 nm tall) and the LC molecules (1-3 nm), with the most likely explanation being non-uniformity in LC pretilt or anchoring in the  $n_e$  direction around these structures. Pretilt is a measure of the angle between the long axis of the LCs and the substrate surface, and changes in pretilt affect the effective refractive index experienced by the incident visible light [31]. Anchoring describes interactions between LC molecules and the substrate surface [32]. For standard LC cells, the pretilt and anchoring are expected to be uniform across the whole substrate. Here, variations are caused by a combination of surface topography, potential variations in PI thickness, and changes in stripe pitch and depth in and around the "C" and "I" structures [33,34].



Due to these variations, when we probe the  $n_e$  direction with polarized white light (Fig. 2(b)), the LCs effectively create regions of varying refractive index. The LCs then act as scattering sites for this polarization of the incident light, which disrupts the coherence of the diffraction pattern, as demonstrated in Fig. 2(c2) and (c3). The pretilt of the aligned LCs has no effect when probing the  $n_o$  direction, evident by the diffraction pattern which matches the bare sample, as the LCs probed in this orientation are uniform from one to another resulting in a clear diffraction pattern. Modelling effects such as pretilt and anchoring of LCs (1 - 3 nm) around structures which are several orders of magnitude larger (unit cell 70 x 80  $\mu\text{m}$ ) becomes very computationally expensive and moves beyond the scope of this report. We are, however, able to use this effect to visually demonstrate the THz field reorienting the LCs through k-space imagery.

### 3. Methods

The THz data presented in this report was acquired using a conventional oscillator-based THz-TDS, illustrated in Fig. 3(a). In this setup, a Ti:Sapphire laser produces 100 femtosecond pulses, at a repetition rate of 80 MHz, with a peak wavelength of 780 nm divided, by a beamsplitter, between two PCAs serving as both the THz emitter and detector. 150 mW femtosecond pulses were used to pump the PCA emitter which produces picosecond pulses, for which the delay line allows us to capture the full time-domain waveform. A Fourier transform of the time-domain gives the frequency spectrum with a bandwidth of 0.1 - 3 THz. The polarized THz pulse is first collimated and focused onto the sample, before recollimation and focusing onto the detector.

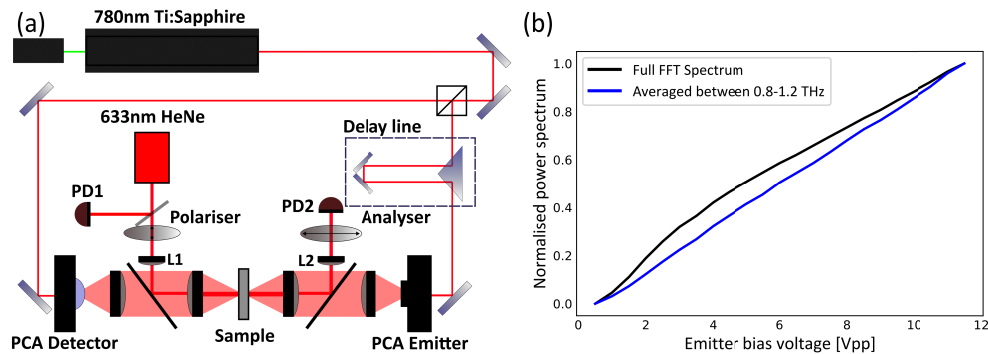


**Fig. 3.** (a) Setup schematic: A mode-locked Ti:Sapphire laser generates 100 femtosecond pulses at a peak wavelength of 780 nm. The pulses are divided by a beamsplitter between two PCAs that serve as both THz emitter and detector. To enable scanning of the full THz time-pulse, a delay line is integrated into the emitter arm. This setup employs a four-lens configuration: the THz beam is emitted by the PCA, collimated, focused through the sample, then collimated once more before being refocused onto the THz detector. A 633 nm HeNe laser beam runs collinear to the THz beam, allowing for the recording of the hybrid cell's visible light transmittance. The 633 nm beam passes through a polarizer and analyzer before measurements are recorded by a photodetector. Lenses L1 and L2 are incorporated to ensure that the optical beam remains collimated as it passes through the sample. Pellicles reflect the visible light into and out of the THz beam path. (b) Power characterization of the PCA emitter for different bias voltages. Characterization was conducted for both the full spectrum (black line) and the MM resonance (blue line). These results were derived from air scans performed using THz-TDS at different bias voltages supplied to the PCA emitter.

The investigation involved changing the DC bias supplied to the PCA emitter, which operates based on principles outlined in [35]. Comprising a semiconductor material and patterned electrodes with a small gap, PCA emitters generate free carriers when exposed to the incident

femtosecond pulse. An external DC bias accelerates these carriers, creating a transient photocurrent dependent on the carrier envelope of the optical pulse and lifetime of the carriers. The lifetime of this photocurrent within the semiconductor is on the order of a few picoseconds, resulting in a THz pulse with an electric field proportional to the change in photocurrent. By controlling the DC bias supplied to our emitter we aim to control the intensity incident upon the hybrid cell.

To characterize the THz intensity, we investigated the impact of reducing the DC bias on the PCA emitter's output by taking THz-TDS scans at different bias voltages. The frequency spectrum was integrated and normalized with the results presented in Fig. 3(b). For the full spectrum (0.1 - 3 THz) there exists non-linear behaviour for low bias voltages, as our signal approaches the noise floor. However, within the MM resonance band (0.8 - 1.2 THz), where the highest signal-to-noise (SNR) exists for our spectrometer, a linear correlation between the power spectrum and emitter bias voltage is observed.

Our investigation also included an optical probe to investigate the degree of LC orientation by measuring the transmittance through a polarizer-analyzer setup. A 633 nm He-Ne laser was introduced collinear to the THz beam (Fig. 3(a)), via lenses L1 and L2, which ensure that the optical beam is collimated through the sample. Collimation of the optical beam through the sample is necessary to eliminate the effect of the individual geometry of the MMs influencing the output of the photodetector. By not focusing the optical beam we can probe a larger area and ensure better uniformity between measurements. The THz beam at focus was found to have a beam radius of 1.51 mm, while the radius of the collimated HeNe was 1.29 mm. Pellicles were used to reflect visible light; these are thin plastic sheets ( $\approx 10\mu\text{m}$ ) that remain transmissive to THz radiation. The two polarizers are configured depending on the mode of the hybrid cell under investigation and the transmittance is recorded by a photodetector (PD2). A second photodetector (PD1) is used as a reference. A CCD camera can also be incorporated to capture the k-space diffraction pattern by replacing PD2 and adding an appropriate lens.

The optical part of this setup is typical of both pixel technology [36] and LC study [37], whereby an external voltage would be supplied to the cell to induce an LC reorientation. Orthogonal polarization components of the incident light will undergo distinct phase delays as it passes through the LC cell, known as birefringence. As a result, the beam output polarization will change leading to variations in transmittance for the voltage scan, as the beam passes the analyzer. These variations depend upon the voltage supplied to the cell and the angle between the optical axis of the LCs,  $\vec{n}$ , and the polarizer axes. In this investigation, we apply no external voltage to the cell. Instead by varying the intensity of incident THz radiation, we leverage the concept that LC reorientation manifests itself as a change in optical transmittance. This allows us to infer that the THz field itself, enhanced in the plane of the MM structure, is responsible for the LC reorientation.

To confirm the role of MM-amplified local THz fields in reorienting LC molecules, we optically investigated the hybrid cell using 633 nm laser light in two modes: the global maximum transmittance mode ( $T_g(\text{max})$ ) and a local minimum transmittance mode ( $T_l(\text{min})$ ). These modes correspond to the polarizer LC configurations shown in Fig. 4. The presence of both typical LC polarization effects and the previously mentioned scattering effect results in both global and local maxima and minima. Typical IPS cells can be configured into two modes: normally white, i.e., an initially maximum transmission mode, or normally black, i.e., an initially minimum transmission mode. These modes can be selected by having the rubbing (alignment) direction of the LCs perpendicular (normally white) or parallel (normally black) to the polarizer/analyzer [38]. In our case, the presence of the scattering effect introduces two new modes: a maximum and minimum transmittance mode for the scattering effect. We chose a local minimum, corresponding to the minimum scattering mode but maximum polarizer mode, rather than a global minimum to maximize the transmittance change due to LC reorientation and

exploit higher SNR. Measurements using the global minimum mode are challenging as very little light reaches PD2, making it difficult to distinguish small changes in transmittance. The global minimum can be achieved by rotating the analyzer 90 degrees in the local  $T_I(\min)$  mode from what is depicted in Fig. 4. The expected optical transmittance for  $T_g(\max)$  and  $T_I(\min)$  when the THz field is off and on are shown in Fig. 4(a) and (b), respectively. To normalize the transmission data in our study, we used the minimum transmittance from the  $T_I(\min)$  mode and the maximum transmittance from the  $T_g(\max)$  mode, both obtained without an incident THz beam.

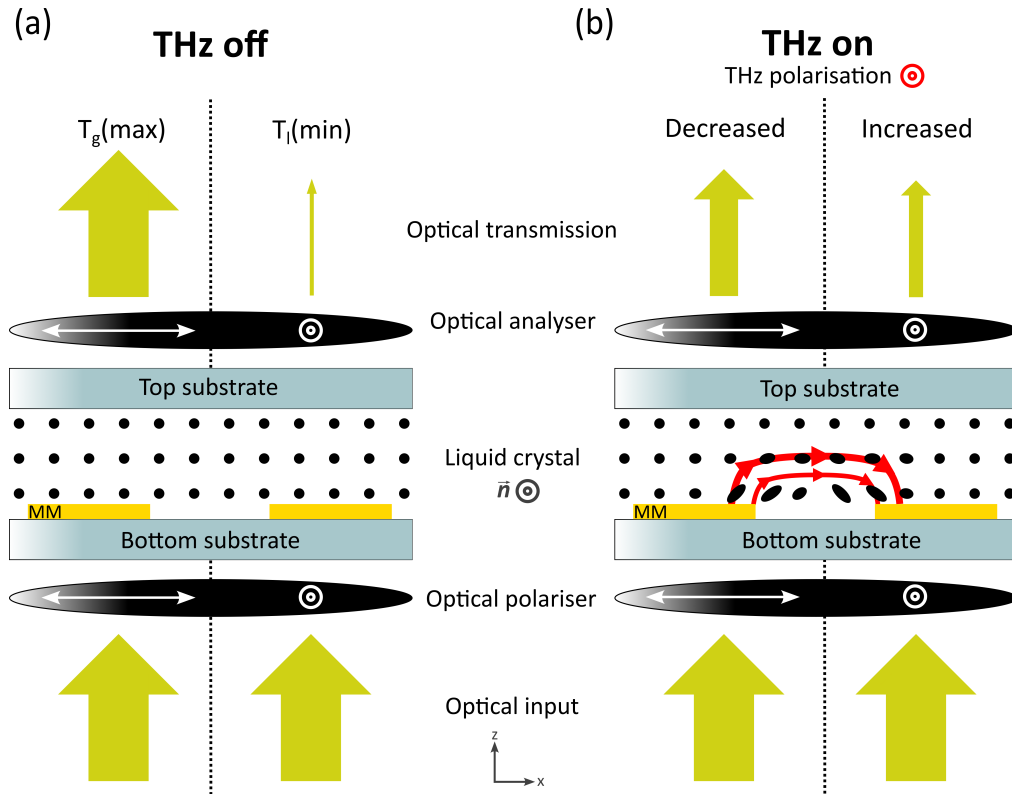


**Fig. 4.** Expected transmission for the 633 nm optical beam (yellow arrows) through the hybrid cell for when: (a) THz field is off and (b) THz field is on. To ensure the THz field is resonant with the MM film, the THz polarization is always incident parallel to the straight sections of the MMs (red target). For the  $T_g(\max)$  mode, corresponding to the maximum scattering mode in Fig. 2(c1), the polarizer axes (white arrows) are set perpendicular to the LC director (black target),  $\vec{n}$ . For the  $T_I(\min)$  mode, corresponding to minimum scattering mode in Fig. 2(c3), the polarizers (white targets) are set parallel to the LC director. When the THz field is incident on the MMs, the amplified in-plane field (denoted by red field arrows) is expected to reorient the LC molecules, resulting in an optical transmission drop for the  $T_g(\max)$  mode and an optical transmission increase for the  $T_I(\min)$ .

#### 4. Results and discussion

The results of this investigation are shown in Fig. 5, where (a) shows how the MM resonance changes with emitter bias voltage referenced against an empty quartz cell of the same thickness. It is clear that as the emitter bias is reduced, the strength of the resonance is also reduced as can be inferred from the flattening of the transmission dip at 0.95 THz. The weakening of the resonance

is highlighted in Fig. 5(b) where the transmission at the dip has been plotted against emitter bias and referenced to a point away from the resonance (0.5 THz). We can see that despite a linear relationship shown in Fig. 3(b) the transmission at the dip does not track linearly with emitter bias. This is because we are dealing with a Kerr-type nonlinear effect, which is 3rd order. Unlike the traditional optical Kerr nonlinearity, which is based on the almost instantaneous build-up of non-linear electric polarization, the effect here is a much slower effect that happens because of molecular rotations caused by the in-plane electric fields of the MMs. This slow  $\chi^3$  effect has been studied in literature [39]. For these reasons, the dependence of the transmittance on the emitter bias (i.e. incident intensity) may well be a cubic function at low incident intensities and should saturate at high incident intensities (large emitter bias). The results for low emitter bias voltages are likely affected by low SNR.

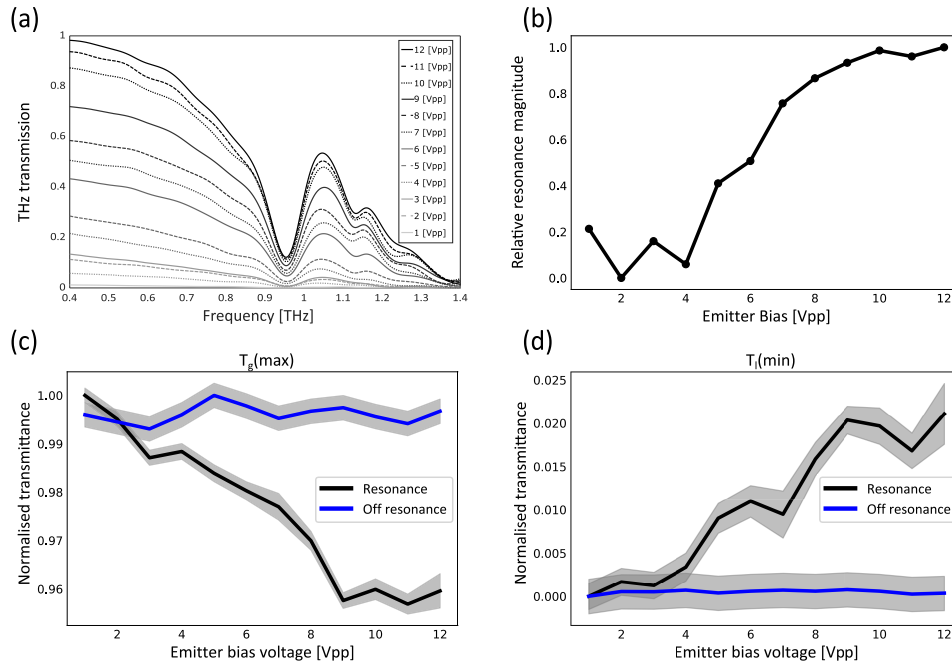


**Fig. 5.** Results for controlling intensity with THz emitter bias (a) THz frequency domain data for the resonant configuration of the hybrid cell for different PCA emitter bias voltages. Scans have been referenced against a 20  $\mu\text{m}$  quartz empty cell. (b) Relative resonance magnitude against PCA emitter bias voltages. Magnitude is obtained by taken the height of the resonance and referencing a point on the frequency spectrum unaffected by the MM resonance (0.5 THz). (c) and (d) are the optical transmittance measurements for the  $T_g(\max)$  mode and  $T_l(\min)$  modes as the PCA emitter bias is changed. The blue lines are the experimental results for the hybrid cell in a non-resonant configuration where no reorientation is expected (i.e., THz polarized orthogonal to straight sections of the metamolecules). The black lines are the experimental results for the resonant configuration where a change in transmittance is expected (i.e., THz polarized parallel to straight sections of the metamolecules). Shaded regions represent the error in measurement before and after a THz-TDS scan was taken.

Based on our simulations, we would expect the resonance to red-shift if an LC reorientation occurs [20]. Our spectrometer, which can resolve up to 20 GHz, was sufficient to observe the maximal shift of 43 GHz when the experimental results were compared to the simulations in a previous investigation [20]. Therefore, as we decrease the emitter bias, we should expect the resonance position to be blue-shifted. However, as the emitter bias decreases, the resonance



becomes broader, and its exact position becomes increasingly difficult to determine due to the low SNR, see Fig. 5(a). It should also be noted that the comparisons in [20] were always made at the highest SNR and maximal LC twist, permitting the 43 GHz shift to be discerned. Here, we investigate incremental reorientation, and for such small changes (a few GHz at a time), we approach the resolution limit of our spectrometer. When close to the resolution limit, artifacts from data processing and windowing also become more prominent [40–42]. Furthermore, our PCAs are optimized for bandwidth rather than power, allowing only a limited viable range of THz powers to be scanned. All of the above make it difficult to determine whether the resonance position is shifting based on the THz data alone.

It is for these reasons we have investigated the hybrid cell with a THz pump optical probe setup, as visible light transmission can be far more sensitive to any LC reorientation. The measured optical data can be found in Fig. 5(c) for the  $T_g(\text{max})$  mode and Fig. 5(d) for the  $T_l(\text{min})$  mode. From the optical data, it is clear that when the MM is resonant with the THz field, a change in optical transmittance occurs as expected in Fig. 4. This is confirmed for both the  $T_g(\text{max})$  and  $T_l(\text{min})$  modes where at low bias voltages a maximum/minimum is observed matching the non-resonant condition, before a decrease/increase in transmittance up to a plateau at around 9 Vpp. Here the enhancement of the THz field by the MM promotes realignment of the LCs to follow the local in-plane fields lines up to a maximum reorientation of  $\frac{\pi}{4}$  [21]. This plateau likely coincides with the same mechanism described by Fig. 5(b). For the non-resonant condition, where the MM orientation is orthogonal to the THz polarization and no amplification occurs, a flat optical transmittance is observed for increasing bias voltage. The results in Fig. 5(c) and (d) have been normalized between the  $T_l(\text{min})$  and  $T_g(\text{max})$  mode of the full 20  $\mu\text{m}$  hybrid cell with no incident THz field. For this reason, the transmittance change is low as in practice we expect LCs to twist in small regions within specific 'hotspots' near the MM resonators and not in the bulk LC layer. We would therefore also expect no cycling through extrema to exist within our transmittance measurements indicated by a maximal phase lag of below  $\pi$  radians. It is possible to calculate the maximum phase lag of such a LC layer using [24]

$$\Delta\phi = \frac{2\pi d\Delta n}{\lambda}, \quad (1)$$

where  $\Delta n$  is the effective birefringence, which for LC 1825 is 0.22 when accounting for the maximum reorientation of  $\frac{\pi}{4}$ .  $d$  is the thickness of LC layer equal to 1  $\mu\text{m}$  [21] and  $\lambda$  is the wavelength of the optical probe. Given the maximum phase lag,  $\Delta\phi$ , of such a layer is 2.1 rad this is consistent with our experimental results.

A potential concern when developing LC devices for THz applications is that due to the wavelength associated with THz radiation (1 THz = 300  $\mu\text{m}$ ), optimising for strong, resonant performance necessitates the use of MM structures that are on the order of hundreds of nanometres in height. Such profiles of MM structures, covered by an LC alignment layer, can lead to non-uniform alignment and the creation of defects during the fabrication process, particularly for more complex MM geometries [43]. As previously stated, the presence of the MM layer in the hybrid cell causes variations in pretilt in the  $n_e$  direction, however, as our structures have a preferred directional symmetry we maintain good directional alignment.

This is because we have utilized the effect that LCs generally follow the symmetry of any structures present. A report on the effect of waveguide grooves on the alignment of LCs suggests that, despite the height of the structures, the LCs follow the geometry of any structures or symmetry they encounter, in this case aligning their long axis parallel to the straight edges of the waveguides [44]. A similar effect was demonstrated using the metasurface layer itself [45,46]. This effect, in addition to the rubbed PI layer, ensures good directional alignment of LCs for our hybrid cells. We can confirm this through the observation of the cell using crossed polarizers, in addition to the observations made in Fig. 2(a), where the absence of stripes when probing the  $n_o$  direction indicates good directional alignment.

Further exploration of these structural/pretilt effects lies beyond the scope of this report and would be more relevant to an investigation into device performance than to understanding the system mechanism. However, we can use this pretilt effect to visibly show the LC reorientation by averaging several k-space images of the resonant and non-resonant conditions (see inset to Fig. 1) and subtracting the THz on images from the THz off states. Figure 6 shows the subtraction between the THz on and THz off states for both the non-resonant (Fig. 6(a)) and resonant conditions (Fig. 6(b)). These images have been taken with the visible light polarizer set at 45 degrees to the MM orientation corresponding to the configuration in Fig. 2(c2). This ensures that we observe the maximal transmittance change if the MM-enhanced THz field induces an LC reorientation. As seen in the resonant condition, there is a significant difference between the on and off states, indicating a change in the diffraction pattern, as expected if an LC reorientation occurs. Very little difference is observed for the non-resonant condition, with any changes likely attributable to laser drift or experimental error between averages. Figure 6 supports our results for the emitter bias, showing that the LCs are being reoriented through the in-plane amplification of the THz field by the MMs. To further understand the mechanism of reorientation we plan to map the local birefringence to measure the pretilt variations. Additionally, we aim to investigate the time dependence of the LC reorientation through further modulation of the THz beam using an optical chopper.

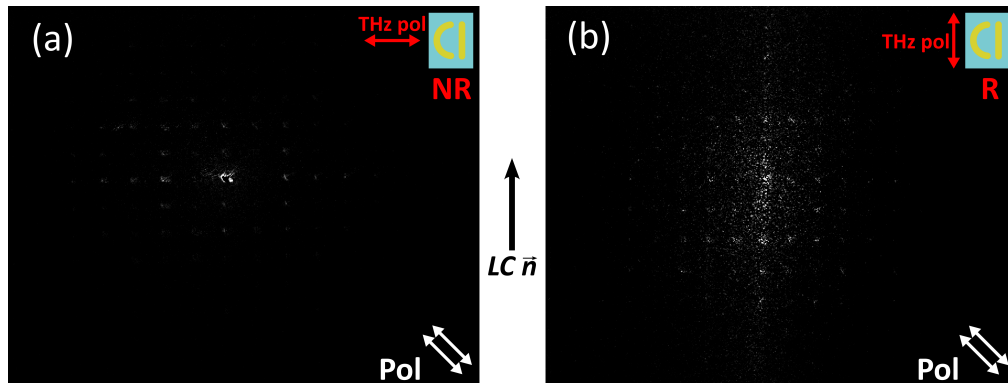


**Fig. 6.** Amplified k-space difference images calculated by averaging several images with the THz field incident on the sample, subtracted from the average of several images with the THz field off for both (a) the non-resonant (NR) mode and (b) the resonant (R) mode. As expected a clear change in the diffraction pattern is observed when in the resonant configuration, while very little difference is seen when in the non-resonant configuration. Insets show the THz polarization (red arrow) relative to the MM orientation. The polarizer and analyzer (white arrows) are colinear and set 45 degrees to the LC director (black arrow) for both difference images. This corresponds to the diffraction pattern in Fig. 2(c2) and where the steepest gradient for transmission change due to LC reorientation exists.

## 5. Conclusions

In this work, we present the first direct experimental evidence that a terahertz field, resonantly amplified in the plane of a metallic metamaterial, can cause liquid crystals to locally reorient from their initial alignment, leading to a strong nonlinear response in the liquid crystal-metamaterial hybrid cell. Using the terahertz beam as a pump and a visible light beam as a probe, we measured the optical transmission through the hybrid cell while it was placed between polarizers. By changing the intensity of the terahertz beam, we were able to show modulation of the optical probing beam's transmission, indicating liquid crystal reorientation. These results were further

confirmed by capturing k-space images of the visible light diffraction pattern using the same configuration. The observed changes in the diffraction pattern provided additional evidence of local reorientation of the liquid crystals induced by the terahertz field. This work, showcasing electrode-free and threshold-free liquid crystal reorientation using low-power terahertz sources, opens up new possibilities for all-optical active applications, including modulators, waveplates, and adaptive lenses. Further, the same concept can enable the study of non-linear interactions between terahertz radiation and other molecular or nanomaterial systems. Additionally, liquid crystal molecules following the local electric field can serve as localized sensors, providing an intuitive mapping of the electric field of a metamaterial and other near-field resonant systems. We plan to maximize this effect through the following routes: (a) optimization of the metamaterial design to improve enhancement and (b) choice of liquid crystal, where a small  $K_2$  elastic constant value will result in a larger angle of twist [21]. Using these methods, we aim to extend the range of nonlinear effects beyond local 'hotspots' into the bulk liquid crystal layer.

**Acknowledgments.** We want to thank Giampaolo D'Alessandro for useful discussion and advice and Eleni Perivolari for their previous contributions to the foundational work on this project.

**Disclosures.** The authors declare no conflicts of interest.

**Data availability.** Data underlying the results presented in this paper are available from the University of Southampton repository at [47].

## References

1. J. F. Federici, B. Schulkin, F. Huang, *et al.*, "Thz imaging and sensing for security applications - explosives, weapons and drugs," *Semicond. Sci. Technol.* **20**(7), S266–S280 (2005).
2. P. Jain, H. Chhabra, U. Chauhan, *et al.*, "Machine learning assisted hepta band thz metamaterial absorber for biomedical applications," *Sci. Rep.* **13**(1), 1792 (2023).
3. M. Gezimatli and G. Singh, "Advances in terahertz technology for cancer detection applications," *Opt. Quantum Electron.* **55**(2), 151 (2023).
4. Y. Fu, X. Fu, S. Yang, *et al.*, "Two-dimensional terahertz beam manipulations based on liquid-crystal-assisted programmable metasurface," *Appl. Phys. Lett.* **123**(11), 111703 (2023).
5. T. Nagatsuma, G. Ducournau, and C. C. Renaud, "Advances in terahertz communications accelerated by photonics," *Nat. Photonics* **10**(6), 371–379 (2016).
6. T. Harter, C. Füllner, J. N. Kemal, *et al.*, "Generalized kramers–kronig receiver for coherent terahertz communications," *Nat. Photonics* **14**(10), 601–606 (2020).
7. A. Leitenstorfer, A. S. Moskalenko, T. Kampfrath, *et al.*, "The 2023 terahertz science and technology roadmap," *J. Phys. D: Appl. Phys.* **56**(22), 223001 (2023).
8. M. Tonouchi, "Cutting-edge terahertz technology," *Nat. Photonics* **1**(2), 97–105 (2007).
9. B. Ferguson and X.-C. Zhang, "Materials for terahertz science and technology," *Nat. Mater.* **1**(1), 26–33 (2002).
10. O. Buchnev, N. Podoliak, K. Kaltenecker, *et al.*, "Metasurface-based optical liquid crystal cell as an ultrathin spatial phase modulator for thz applications," *ACS Photonics* **7**(11), 3199–3206 (2020).
11. O. Buchnev, J. Wallauer, M. Walther, *et al.*, "Controlling intensity and phase of terahertz radiation with an optically thin liquid crystal-loaded metamaterial," *Appl. Phys. Lett.* **103**(14), 141904 (2013).
12. Y. Wen, Y. Qi, L. Wang, *et al.*, "Dynamically switchable multifunctional terahertz absorber based on graphene and vanadium dioxide hybrid metamaterials," *J. Opt. Soc. Am. B* **40**(3), 509 (2023).
13. Z. Zheng, Y. Luo, H. Yang, *et al.*, "Thermal tuning of terahertz metamaterial absorber properties based on  $\text{VO}_2$ ," *Phys. Chem. Chem. Phys.* **24**(15), 8846–8853 (2022).
14. P. Pitchappa, A. Kumar, S. Prakash, *et al.*, "Chalcogenide phase change material for active terahertz photonics," *Adv. Mater.* **31**(12), 1808157 (2019).
15. K. Chen, W. Song, Z. Li, *et al.*, "Chalcogenide phase-change material advances programmable terahertz metamaterials: a non-volatile perspective for reconfigurable intelligent surfaces," *Nanophotonics* **13**(12), 2101–2105 (2024).
16. S. T. Xu, H. F. Zhang, L. Cong, *et al.*, "Dispersion-compensated terahertz ultra-broadband quarter and half wave plates in a dielectric-metal hybrid metadevice," *Adv. Opt. Mater.* **12**(13), 2302696 (2024).
17. Y. Huang, Y. Lan, S. Zhong, *et al.*, "Design of tunable dual-band terahertz metamaterial absorber with liquid crystal integrated on-chip," *IEEE Transactions on Plasma Science* **52**(10), 4993 (2024).
18. S.-T. Xu, J. Fan, Z. Xue, *et al.*, "Terahertz polarization conversion and asymmetric transmission based on a liquid crystal integrated eit metasurface," *Opt. Lett.* **49**(17), 4891 (2024).
19. S. Wang, H. Guo, B. Chen, *et al.*, "Electrically active terahertz liquid-crystal metasurface for polarization vortex beam switching," *Laser Photonics Rev.* **18**(7), 2301301 (2024).
20. E. Perivolari, V. A. Fedotov, J. Parka, *et al.*, "Anomalous resonance frequency shift in liquid crystal-loaded thz metamaterials," *Nanophotonics* **11**(10), 2341–2348 (2022).

21. B. Beddoes, E. Perivolari, M. Kaczmarek, *et al.*, “All-optical switching of liquid crystals at terahertz frequencies enabled by metamaterials,” *Opt. Express* **31**(11), 18336 (2023).
22. J. Neu and C. A. Schmittenmaer, “Tutorial: An introduction to terahertz time domain spectroscopy (thz-tds),” *J. Appl. Phys.* **124**(23), 231101 (2018).
23. M. Reuter, N. Vieweg, B. M. Fischer, *et al.*, “Highly birefringent, low-loss liquid crystals for terahertz applications,” *APL Mater.* **1**(1), 012107 (2013).
24. D. Bankova, N. Brouckaert, N. Podoliak, *et al.*, “Characterisation of liquid crystals in optically thin cells,” *Appl. Opt.* **61**(16), 4663–4669 (2022).
25. F. Khoshkhati, M. Mohammadimasoudi, S. N. Hosseini, *et al.*, “Optimizing liquid crystal cell thickness in electro-optical fresnel lenses through theoretical calculations and experimental validation,” *Opt. Express* **31**(13), 21407 (2023).
26. V. Fedotov, *Metamaterials* (Springer International Publishing, 2017), pp. 1351–1377.
27. K. Koshelev, S. Lepeshov, M. Liu, *et al.*, “Asymmetric metasurfaces with high- $q$  resonances governed by bound states in the continuum,” *Phys. Rev. Lett.* **121**(19), 193903 (2018).
28. S.-T. Xu, J. Fan, Z. Xue, *et al.*, “Active control of terahertz quasi-bic and asymmetric transmission in liquid crystal integrated metasurface,” *Photonics Res.* **12**(10), 2207–2213 (2024).
29. J. Gersten and A. Nitzan, “Electromagnetic theory of enhanced Raman scattering by molecules adsorbed on rough surfaces,” *The J. Chem. Phys.* **73**(7), 3023–3037 (1980).
30. A. V. Ermushev, B. V. Mchedlishvili, V. A. Oleinikov, *et al.*, “Surface enhancement of local optical fields and the lightning-rod effect,” *Quantum Electron.* **23**(5), 435–440 (1993).
31. V. Belyaev, A. Solomatin, D. Chausov, *et al.*, “Orientation effects in nematic liquid crystals in electric and magnetic fields,” *Sov. Phys. Crystallogr.* **7**, 349–354 (2004).
32. E. Perivolari, G. D’Alessandro, V. Apostolopoulos, *et al.*, “Two-dimensional snapshot measurement of surface variation of anchoring in liquid crystal cells,” *Liq. Cryst.* **48**(15), 2086–2096 (2021).
33. D. R. Chiou, L. J. Chen, and C. D. Lee, “Pretilt angle of liquid crystals and liquid-crystal alignment on microgrooved polyimide surfaces fabricated by soft embossing method,” *Langmuir* **22**(22), 9403–9408 (2006).
34. W.-Y. Wu, C.-C. Wang, and A. Y.-G. Fuh, “Controlling pre-tilt angles of liquid crystal using mixed polyimide alignment layer,” *Opt. Express* **16**(21), 17131–17137 (2008).
35. P. Smith, D. Auston, and M. Nuss, “Subpicosecond photoconducting dipole antennas,” *IEEE J. Quantum Electron.* **24**(2), 255–260 (1988).
36. M. Schadt, H. Seiberle, and A. Schuster, “Optical patterning of multi-domain liquid-crystal displays with wide viewing angles,” *Nature* **381**(6579), 212–215 (1996).
37. T. Bennett, M. Proctor, M. Kaczmarek, *et al.*, “Lifting degeneracy in nematic liquid crystal viscosities with a single optical measurement,” *J. Colloid Interface Sci.* **497**, 201–206 (2017).
38. H. Hong, *In-Plane Switching (IPS) Technology* (Springer Berlin Heidelberg, 2012), pp. 1469–1483.
39. P. Salén, M. Basini, S. Bonetti, *et al.*, “Matter manipulation with extreme terahertz light: Progress in the enabling thz technology,” *Phys. Rep.* **836–837**, 1–74 (2019).
40. A. Rehn, D. Jahn, J. C. Balzer, *et al.*, “Periodic sampling errors in terahertz time-domain measurements,” *Opt. Express* **25**(6), 6712 (2017).
41. J. Vázquez-Cabo, P. Chamorro-Posada, F. J. Fraile-Peláez, *et al.*, “Windowing of thz time-domain spectroscopy signals: A study based on lactose,” *Opt. Commun.* **366**, 386–396 (2016).
42. J. Xu, T. Yuan, S. Mickan, *et al.*, “Limit of spectral resolution in terahertz time-domain spectroscopy,” *Chin. Phys. Lett.* **20**(8), 1266–1268 (2003).
43. B. Atorf, H. Mühlenbernd, M. Muldarisnur, *et al.*, “Effect of alignment on a liquid crystal/split-ring resonator metasurface,” *ChemPhysChem* **15**(7), 1470–1476 (2014).
44. Y. Atsumi, K. Watabe, N. Uda, *et al.*, “Initial alignment control technique using on-chip groove arrays for liquid crystal hybrid silicon optical phase shifters,” *Opt. Express* **27**(6), 8756 (2019).
45. O. Buchnev, J. Y. Ou, M. Kaczmarek, *et al.*, “Electro-optical control in a plasmonic metamaterial hybridised with a liquid-crystal cell,” *Opt. Express* **21**(2), 1633–1638 (2013).
46. X. Chang, M. Pivnenko, A. Singh, *et al.*, “Dielectric meta-atoms with liquid crystal alignment effect for electrically tunable metasurface,” *Adv. Devices & Instrum.* **5**, 0040 (2024).
47. B. Beddoes, N. Klokou, M. Kaczmarek, *et al.*, “Dataset for “Making liquid crystals twitch under metamaterial-enhanced terahertz illumination: toward strong optical nonlinearity,”” University of Southampton (2025), <https://doi.org/10.5258/SOTON/D3334>.